Numerical calculation of classical bremsstrahlung

Longhuan Kim and R. H. Pratt
Department of Physics and Astronomy, University of Pittsburgh, Pittsburgh, Pennsylvania 15260
(Received 31 October 1986)

We have carried out numerical calculations for the classical bremsstrahlung spectrum, angular distribution, and polarization resulting from electrons scattering in screened atomic potentials. The calculations utilize the classical theory of electromagnetic radiation from moving charges together with the classical mechanics of energy-loss-free orbits of charged particles in such potentials. The trajectories of incident electrons in the given central potential are calculated numerically, and the doubly differential bremsstrahlung cross section is obtained by taking the Fourier transform of the acceleration of the dipole moment of the projectile and integrating the radiation over the impact parameters of the beam. Results have been obtained for several neutral atoms for electron energies from 1 eV to 500 keV, using self-consistent Dirac-Slater atomic potentials. Comparisons with quantum-mechanical partial-wave results for the spectrum show that, as in the point Coulomb case, the classical method is generally good for screened potentials for low incident electron energies. The classical method therefore can be useful in low-energy situations for which the usual Elwert-Born form-factor method is not satisfactory. We have also obtained and examined the angular distributions of classical bremsstrahlung. Screening reduces the value of the asymmetry parameter which characterizes the angular distribution of dipole radiation. The difference of screened results from the point Coulomb results increases with decreasing incident electron energy. At very low energy the value of the asymmetry parameter oscillates with energy, and this also leads to oscillations in the degree of polarization.

I. INTRODUCTION

In this paper we present calculations of the bremsstrahlung process from isolated neutral atoms using a classical method. The bremsstrahlung process as treated in a static potential is fairly well understood, and in many situations an accurate theoretical description of the resulting radiation can be obtained. Accurate predictions for bremsstrahlung spectra and angular distributions from relativistic partial-wave calculations for selected energies and target elements have been published.[1,2] Tables of bremsstrahlung spectra and angular distributions interpolated from these results are also available.[3] However these tables do not provide data for electron energies lower than 1 keV, which is basically the lower limit of the energy range for which the code was designed. While a code could be written for lower energies, the existing data suggests that simpler methods may suffice.

Several simple approximations are available to calculate bremsstrahlung cross sections. Some analytic expressions are available for bremsstrahlung from a point Coulomb potential, and Born approximation provides a simple prediction for the effect of screening. Among these approaches are the classical Coulomb formula,[4] nonrelativistic quantum-mechanical dipole approximation for the Coulomb potential,[5] nonrelativistic Born approximation and Elwert-Born form-factor method,[6,7] and relativistic Born approximation.[8] These simple approaches are useful not only because they give appropriate predictions for the bremsstrahlung cross sections in certain situations, but also because they help us to understand the features of bremsstrahlung, tracing the origins of the properties of the process.

For the point Coulomb potential fairly accurate results can be obtained using these simple approximations appropriately.[9–11] For screened potentials the Elwert-Born form-factor method is available. However, this method does not apply to the low-energy case, for which numerical quantum-mechanical partial-wave calculations are unavailable. Such calculations would be complicated and expensive.

The classical method is known to give accurate results for low-energy bremsstrahlung in the point Coulomb case.[12] This approach is based on the classical motion of electrons in the scattering field and the classical electromagnetic theory of radiation. Electrons coming into the atomic field are accelerated by the Coulomb force of the field and hence emit bremsstrahlung radiation. The motion of each electron can be determined precisely from the classical dynamics. The intensity, the spectrum, and the angular distribution of the radiation can then be determined from classical electrodynamics.

Important early work on classical bremsstrahlung in electron-atom scattering is due to Kramers.[4] He obtained the bremsstrahlung spectrum (the cross-section differential in radiation frequency) in closed form for hydrogenic atoms. His method assumes that the loss of electron kinetic energy due to the radiation is negligible and therefore does not affect the electron trajectory. This method also omits retardation and does not contemplate multipole radiation. Relativistic effects on the electron motion are also normally neglected.

With the help of modern computers it is possible, under the same assumptions, to carry out full numerical calculations of the classical bremsstrahlung for screened poten-

tials. The validity of the classical method in the screened case has been unclear. As far as we know there has been no work on the numerical calculation of classical bremsstrahlung for screened potentials.

Recently, we have developed a computer code (CLB) to calculate the spectra and angular distributions of classical bremsstrahlung for electrons scattering from screened atomic potentials. The code calculates numerically the trajectory of an incident electron in a central potential according to classical dynamics. The radiation spectrum from a trajectory is obtained from the Fourier transform of the dipole moment of the electron on that trajectory. The total radiation spectrum is then obtained by integrating the spectrum over all trajectories. In this calculation we neglect the effect of energy loss due to the radiation. Higher multipole radiation and retardation effects are also omitted.

The code is designed to accept numerical potentials as input; in our work we have generally utilized self-consistent Dirac-Slater potentials with Kohn-Sham exchange energies, which well characterize a neutral atom. The incident electron kinetic energy ranges we considered in this calculation are from 1 eV to 1 MeV, depending on the atomic number of the target atom.

Features of classical bremsstrahlung from a screened potential are discussed in terms of our results. The validity of classical results in the screened case is examined by comparing with available quantum-mechanical results. It is found that, for low-energy bremsstrahlung, the classical method is also good in the screened case (as well as the Coulomb case) and gives better results than the form-factor method. Thus this method can provide a simpler way to obtain the spectrum and distribution of low-energy bremsstrahlung, where screening is too important to be neglected. For high energy, the classical method fails to give correct absolute cross sections, but it still can be useful in predicting the ratio of the screened result to the Coulomb result, providing probably an easier way to obtain exact screened results from exact Coulomb results.

It should be noticed that the range of validity of classical results is much wider than may be anticipated. Jackson,[13] for example, describes the classical spectrum as confined to very low frequencies, for quanta of energy low compared to the incident electron kinetic energy. However, this results from the consideration only of small-angle scattering (small momentum transfer); higher frequencies are radiated in larger-angle scattering, as in Kramers's original work. With our numerical calculation, which considers all possible momentum transfers, we find that, for low incident electron energy, classical results for the spectrum can be valid in the entire range of the spectrum.

Our results for the angular distribution show a rather complicated phenomenon. The asymmetry parameters for screened potentials are increasingly reduced from the Coulomb values with decreasing electron incident energy. However, below a certain energy the asymmetry parameter begins to increase rapidly with decreasing energy and then oscillates. This phenomenon is related to the large scattering angles possible for electrons in a screened Coulomb potential.

We begin in Sec. II with the basic formalism of classical bremsstrahlung and a description of our numerical method. In Sec. III we present our results for spectra and discussions of their features and validity. In Sec. IV we present results and discussions for the angular distributions. In this section we also discuss the polarization of the bremsstrahlung radiation.

II. DESCRIPTION OF THE METHOD

The intensity of dipole radiation from a charge system emitted into a solid angle $d\Omega$, in a direction $\hat{\mathbf{n}}$, is given by the expression[14] (we use natural units, i.e., $m_e=c=\hbar=1$)

$$dE(t)=\frac{[\ddot{\mathbf{d}}(t)\times\mathbf{n}]^2}{4\pi}d\Omega\ , \tag{1}$$

where $\mathbf{d}$ is the electric dipole moment of the system, and $\ddot{\mathbf{d}}$ is the second time derivative of $\mathbf{d}$.

For the electron-atom scattering problem, we consider a beam of electrons of unit current passing through the potential field of an atom. The electrons are accelerated in the potential and it is this acceleration which leads to radiation. Because the scattering field is spherically symmetric and the incident beam is parallel, the scattering, also the radiation, has axial symmetry about an axis in the direction of the beam passing through the scattering center. We choose this axis as the z axis. The x axis is chosen so that $\mathbf{n}$ is in the x-z plane [Fig. 1(a)].

Consider an electron coming into the field. Because of the spherical symmetry of the potential the entire trajectory will be in a plane 0-x_1,z determined by the impact parameter $\boldsymbol{\rho}$ (which is perpendicular to the z axis) and the z axis [Fig. 1(b)]. For a given potential and given incident energy, the trajectory of an incident electron is fully determined by the impact parameter, either in terms of nonrelativistic or relativistic dynamics. Note that in this usual treatment the energy loss due to radiation is not considered in determining trajectories. The intensity of the radiation from one electron is determined by Eq. (1) with $\mathbf{d}=-e\mathbf{r}$, where $-e$ is the electron charge. The total radiation emitted in the direction $\mathbf{n}$ from all electrons is then obtained by integrating Eq. (1) over all electrons in the beam. This is done by first taking the average of the quantity $(\ddot{\mathbf{d}}\times\mathbf{n})^2$ for all electrons having the same magnitude of impact parameter, then integrating over the magnitude of the impact parameter from 0 to ∞. Since $(\ddot{\mathbf{d}}\times\mathbf{n})^2=\ddot{\mathbf{d}}^2-(\mathbf{n}\cdot\ddot{\mathbf{d}})^2$, only $(\mathbf{n}\cdot\ddot{\mathbf{d}})^2$ is affected by the averaging process. Again, because of the symmetry, it is obvious that the terms $\ddot{d}_z\ddot{d}_y$, $\ddot{d}_x\ddot{d}_z$, and $\ddot{d}_x\ddot{d}_y$ will vanish when averaged. We also have $\langle\ddot{d}_x^2\rangle=\langle\ddot{d}_y^2\rangle=(\ddot{\mathbf{d}}^2-\ddot{d}_z^2)/2$. This yields[14]

$$\overline{(\ddot{\mathbf{d}}\times\mathbf{n})^2}=\tfrac{1}{2}(\ddot{\mathbf{d}}^2+\ddot{d}_z^2)+\tfrac{1}{2}(\ddot{\mathbf{d}}^2-3\ddot{d}_z^2)\cos^2\theta\ , \tag{2}$$

and the radiation distribution is then

$$\frac{dE(t)}{d\Omega}=\frac{1}{4\pi}\int_0^\infty[\tfrac{2}{3}\ddot{\mathbf{d}}^2+\tfrac{1}{3}(\ddot{\mathbf{d}}^2-3\ddot{d}_z^2)P_2(\cos\theta)]2\pi\rho\,d\rho\ , \tag{3}$$

where θ is the angle between $\mathbf{n}$ and the z axis, P_2 is the Legendre polynomial of second order $P_2(x)=(3x^2-1)/2$.

In electron-atom scattering problems the radiation in-

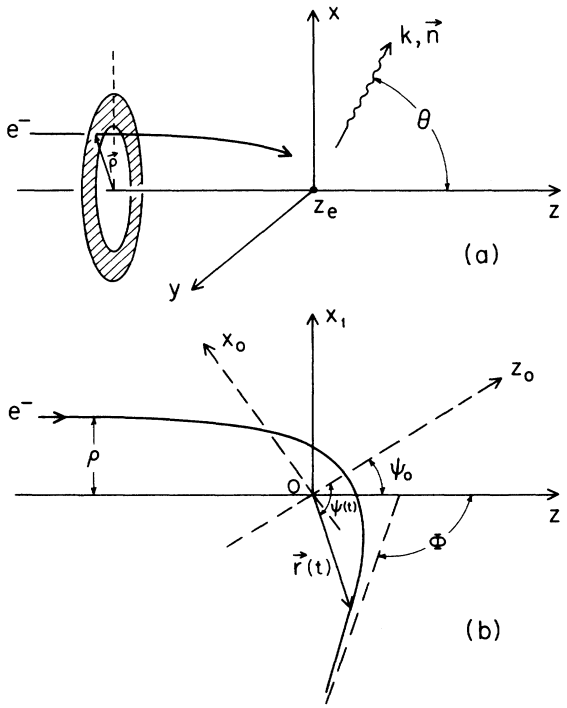

FIG. 1. Geometry of classical bremsstrahlung.

tensity is usually described by the doubly differential cross section $kd^2\sigma/d\Omega\, dk$, the radiation in the frequency interval between k and $k+dk$ emitted into the solid angle $d\Omega$ per unit density of the target per unit current density. This quantity has the dimension of area. The cross section for the radiation of a given frequency emitted in a given direction can be obtained by taking the Fourier transform of the dipole moment, defined as

$$\mathbf{d}_k = \int_{-\infty}^{+\infty} \mathbf{d}(t) e^{ikt} dt \ , \tag{4}$$

where k is the frequency of the radiation. Then the doubly differential cross section can be obtained by replacing $\ddot{\mathbf{d}}$ and $\ddot{d}_z$ by their Fourier components $\ddot{\mathbf{d}}_k$ and $\ddot{d}_{kz}$ in Eq. (3) and multiplying by 4π. The result is

$$\frac{kd^2\sigma}{d\Omega dk} = A + \tfrac{1}{2}BP_2(\cos\theta) \ , \tag{5}$$

with

$$A = \frac{2k^4}{3}\int_0^\infty 2\pi\rho\, d\rho \,|\, \mathbf{d}_k(\rho)\,|^2 \ , \tag{6}$$

$$B = \frac{2k^4}{3}\int_0^\infty 2\pi\rho\, d\rho[\,|\,\mathbf{d}_k(\rho)\,|^2 - 3\,|\,d_{kz}(\rho)\,|^2] \ . \tag{7}$$

Here we used the fact that $\ddot{\mathbf{d}}_k = -k^2\mathbf{d}_k$.

It should be noticed that the second term in Eq. (5) vanishes after integration over angles of radiation emission. The bremsstrahlung energy spectrum, the total radiation within the frequency interval dk, is given by

$$\frac{kd\sigma}{dk} = \frac{8\pi}{3}k^4\int_0^\infty 2\pi\rho\, d\rho \,|\, \mathbf{d}_k(\rho)\,|^2 = \int_0^\infty A_1(\rho)d\rho \ , \tag{8}$$

with

$$A_1(\rho) = \frac{16\pi^2k^4}{3}\rho\,|\,\mathbf{d}_k(\rho)\,|^2 \ . \tag{9}$$

Here $A_1(\rho)d\rho$ represents the contribution to the spectrum from electrons with impact parameters between ρ and $\rho+d\rho$.

The angular distribution of radiation of electron bremsstrahlung from a central potential can also be described in terms of the shape function

$$S(Z,T_1,k,\theta) = \left[\frac{kd^2\sigma}{dkd\Omega_k}\right] \Big/ \left[k\frac{d\sigma}{dk}\right] \ . \tag{10}$$

Comparing Eqs. (5), (6), and (8) we have, for dipole radiation, that

$$S(Z,T_1,k,\theta) = \frac{1}{4\pi}\left[1 + \frac{a_2(Z,T_1,k)}{2}P_2(\cos\theta)\right] \ , \tag{11}$$

where $a_2 = B/A$ is the so-called asymmetry parameter (in some work it is called the "particle parameter"[15]). This parameter characterizes (in dipole approximation) the shape function.

We may also discuss the polarization properties of the radiation. The intensity of the radiation from a given electron can be decomposed into two parts. One part is polarized in the x-z plane (we will call this parallel polarization or x-z polarization) and another part is polarized in the direction perpendicular to the x-z plane (we will call this perpendicular polarization or y polarization.) Both components are perpendicular to the vector $\mathbf{n}$. The electric field vector at distance R_0 is

$$(\ddot{\mathbf{d}}\times\mathbf{n})\times\mathbf{n}/R_0 = [\mathbf{n}(\ddot{\mathbf{d}}\cdot\mathbf{n}) - \ddot{\mathbf{d}}]/R_0 \ . \tag{12}$$

Since $n_y = 0$, the y component of Eq. (12) is $-\ddot{d}_y/R_0$. The intensity of the radiation in the direction of $\mathbf{n}$, with its electric field vector in the y direction, is determined by the mean square $\langle \ddot{\mathbf{d}}_y^2 \rangle = (\ddot{\mathbf{d}}^2 - \ddot{d}_z^2)/2$. For the cross section with such polarization we obtain

$$\frac{kd^2\sigma^{\rm per}}{d\Omega\, dk} = \tfrac{1}{2}\int_0^\infty (\ddot{\mathbf{d}}_k^2 - \ddot{d}_{kz}^2)2\pi\rho\, d\rho \ . \tag{13}$$

The other component can then be obtained using $\sigma = \sigma^{\rm par} + \sigma^{\rm per}$:

$$\frac{kd^2\sigma^{\rm par}}{d\Omega\, dk} = \tfrac{1}{2}\int_0^\infty [\tfrac{1}{3}\ddot{\mathbf{d}}_k^2 + \ddot{d}_{kz}^2 + \tfrac{2}{3}(\ddot{\mathbf{d}}_k^2 - 3\ddot{d}_{kz}^2)P_2(\cos\theta)]2\pi\rho\, d\rho \ . \tag{14}$$

Equations (13) and (14) can be rewritten in terms of the quantities A and B of Eqs. (6) and (7):

$$\frac{kd^2\sigma^{\rm per}}{d\Omega\, dk} = \tfrac{1}{2}(A + \tfrac{1}{2}B) \ , \tag{15}$$

$$\frac{kd^2\sigma^{\rm par}}{d\Omega\, dk} = \tfrac{1}{2}[A - \tfrac{1}{2}B + BP_2(\cos\theta)] \ . \tag{16}$$

Thus the perpendicular component is isotropic while the parallel component has an angular dependence entering through $P_2(\cos\theta)$. Usually the degree of polarization is

represented in terms of a parameter P defined as

$$P=\frac{\frac{d^2\sigma^{\rm par}}{d\Omega\,dk}-\frac{d^2\sigma^{\rm par}}{d\Omega\,dk}}{\frac{d^2\sigma^{\rm per}}{d\Omega\,dk}+\frac{d^2\sigma^{\rm par}}{d\Omega\,dk}} . \tag{17}$$

In our case

$$P=\frac{B-BP_2(\cos\theta)}{2A+BP_2(\cos\theta)}=\frac{1-P_2(\cos\theta)}{2/a_2+P_2(\cos\theta)} . \tag{18}$$

The polarization is directly related to the shape function through the asymmetry parameter a_2. Thus determining both the shape function and the polarization reduces to the problem of determining the asymmetry parameter.

Our discussion so far is valid for all central potentials. To obtain the bremsstrahlung spectrum or the angular distribution for electrons scattering from a particular potential of interest, one needs to evaluate the trajectories of the electrons in that potential. The equation of motion for electrons in a central potential $V(r)$ can be derived from energy and angular momentum conservation:

$$\tfrac{1}{2}\dot{r}^2+\tfrac{1}{2}r^2\dot{\psi}^2+V(r)=T_1 , \tag{19}$$

where $\dot{\psi}$ is the angular velocity. The second and third terms can be combined to form an effective radial potential $V_{\rm eff}$. The radial motion of electrons is then determined from the following equation:

$$\dot{r}=2^{1/2}[T_1-V_{\rm eff}(L,r)]^{1/2},\quad V_{\rm eff}\equiv V(r)+\frac{\mathbf{L}^2}{2r^2} , \tag{20}$$

where $\mathbf{L}$ is the angular momentum, $\mathbf{L}^2=r^4\dot{\psi}^2=2T_1\rho^2$ with ρ the impact parameter. There is a minimum distance r_0 (corresponding to $dr/dt=0$) which an electron of given kinetic energy and angular momentum can reach in a given potential. This distance is called the classical turning point. For screened atomic potentials there can be a barrier and a inner well in the effective potential $V_{\rm eff}$,[16] depending on the angular momentum (i.e., on the initial velocity and impact parameter), present for angular momentum less than some limit (but nonzero). For electrons with energy T_1 lower than a certain limit, it is consequently possible that an electron with proper impact parameter reaches exactly the top of the barrier at $r=r_0$. In this case both dr/dt and $dV_{\rm eff}/dr$ vanish simultaneously at the point. An electron will stay in this unstable circular orbit until a perturbation occurs. This is called a classical resonance. In our present work we do not treat these resonances. The highest energy for which a resonance can occur depends on the potential. In the self-consistent Dirac-Slater potential which we use the energy limit for the resonance is about 0.5 eV for $Z=13$, 30 eV for $Z=47$, and 40 eV for $Z=79$. All the energies we consider are above these resonance energies. Study of the resonance region would clearly be an interesting future subject for investigation.

The scattering angle Φ, defined as the angle between the directions of initial and final velocity of the scattering electron, is determined from the expression

$$\Phi=\int_{r_0}^{\infty}\frac{2\rho\,dr}{r[r^2-\rho^2-r^2V(r)/T_1]^{1/2}}-\pi . \tag{21}$$

For electrons scattering from an attractive point Coulomb field the scattering angle can be calculated analytically:

$$\Phi=2\arcsin\left[\left(\frac{Z\alpha}{2T_1\rho}\right)\Big/(1+Z^2\alpha^2/4T_1^2\rho^2)^{1/2}\right] . \tag{22}$$

The trajectories in the point Coulomb case are all hyperbolic. Mathematically there is a singular case when the impact parameter is exactly equal to zero. The trajectory for this case would be a straight line passing through the origin. However, this straight-line orbit does not contribute to the cross section since the area in impact-parameter space associated with this orbit is zero. Note that this singular orbit is not the limiting orbit for $\rho\to 0$. The limiting value of the scattering angle Φ for $\rho\to 0$ is not zero but π. In Fig. 2(a) we show the scattering orbits and the scattering angle as function of the impact parameter. The scattering angle begins with $\Phi=180°$ at $\rho=0$ (we mean the limiting value of Φ when $\rho\to 0$) and decreases monotonically as ρ increases.

In the screened case the scattering angle Φ is still determined by Eq. (21) but the solution has to be obtained with numerical methods. In Fig. 2(b) we show the orbits of electrons scattering from the charge distribution of a neutral aluminum atom. The Dirac-Slater potential is used to describe the static potential field. The scattering angle for $\rho\to 0$ is the same as in the point Coulomb case, i.e., $\Phi=180°$. In neutral atom potentials at low electron energies, with increasing impact parameters, Φ initially increases, unlike the point Coulomb case where Φ decreases as ρ increases. Φ increases to a maximum value and then it decreases to zero as ρ goes to infinity (or beyond the range of potential). Very-low-energy electrons can make several turns around the field before escaping.[16,17] The scattering angle changes rapidly with impact parameter close to the value for which the maximum scattering occurs. This rapid change of scattering angle plays an important role in the angular distribution of the radiated spectrum in circumstances when most contributions to the spectrum come from such orbits. We will discuss this in Sec. IV.

Our computer code CLB is designed to calculate the doubly differential cross section of classical bremsstrahlung in both the point Coulomb and the screened central potential. This is a numerical code. All important steps of the calculation are done numerically. The central potential is prepared separately and input to CLB as numerical data. The electron trajectories for selected impact parameters are calculated by integrating the equation of motion. Then one takes a numerical Fourier transform of the acceleration $\ddot{\mathbf{r}}$. For a given potential and given incident electron energy, the electron trajectory is determined in full by the impact parameter. Neglecting energy loss by radiation, the outgoing electron has the same energy as the incoming electron.

Due to the spherical symmetry of the potential, each trajectory is symmetric about an axis which is perpendicular to the trajectory at the point of closest approach to the center of the potential. We denote this symmetry axis as the 0-z_0 axis [see Fig. 1(b)]. It is obvious that in the coordinate system 0-x_0,z_0 only half of the trajectory needs to

be evaluated. In the CLB code the calculation starts from $r(t=0)=r_0$, $\psi(t=0)=0$, where ψ is the angle of $\mathbf{r}$ from the z_0 axis as illustrated in Fig. 1(b). The starting distance r_0 is calculated from energy and angular momentum conservation using the equation

$$(\rho/r_0)^2=1-V(r_0)/T_1 \ . \tag{23}$$

The fourth-order Runge-Kutta method is used in evaluating subsequent values of r and ψ as functions of time t. The required Fourier transform is done for $\ddot{\mathbf{r}}(t)$ instead of for $\mathbf{r}(t)$ to take advantage of the fact that $\ddot{\mathbf{r}}\rightarrow\mathbf{0}$ for large r and $\ddot{\mathbf{r}}=(-dV/dr)(\mathbf{r}/r)$. Because of the symmetry, the x component of the Fourier transform has only an imaginary part and the z component only a real part,

$$\ddot{d}_{x0}(k)=-2ie\int_0^\infty \ddot{x}_0(t)\sin(kt)dt$$
$$=2ie\int_0^\infty \frac{dV(r(t))}{dr(t)}\sin\psi(t)\sin(kt)dt \ , \tag{24}$$
$$\ddot{d}_{z0}(k)=-2e\int_0^\infty \ddot{z}_0(t)\cos(kt)dt$$
$$=2e\int_0^\infty \frac{dV(r(t))}{dr(t)}\cos\psi(t)\cos(kt)dt \ . \tag{25}$$

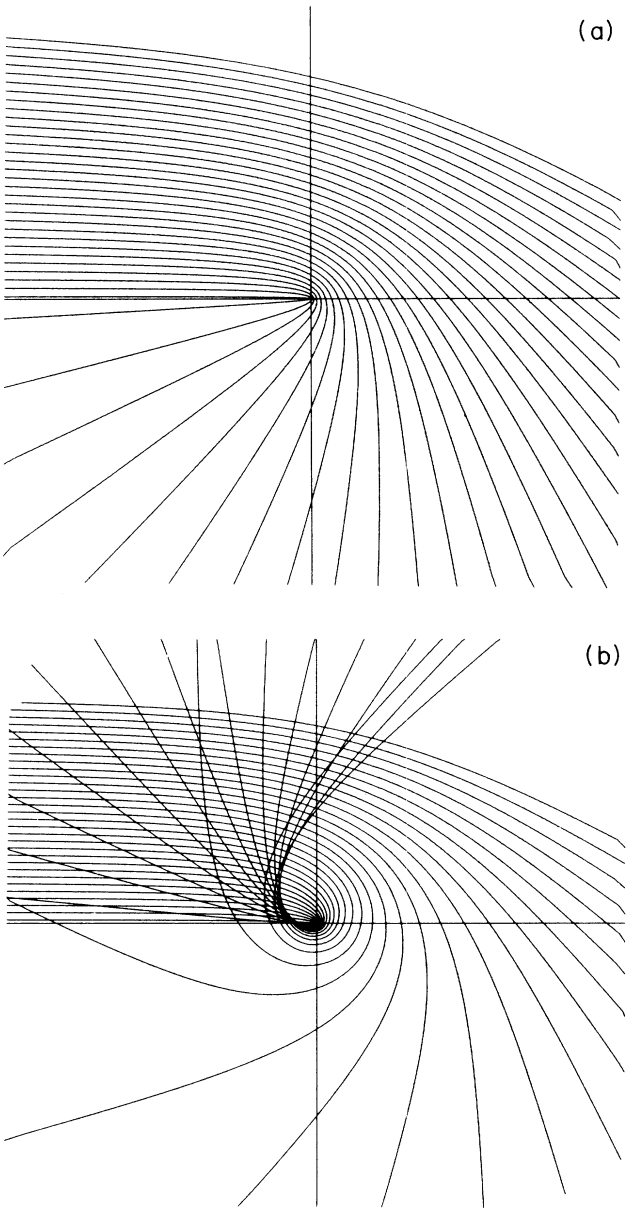

FIG. 2. Electron trajectories at various impact parameters ρ for (a) the point Coulomb potential, (b) a screened potential. In a screened potential the scattering angle Φ is π for $\rho=0$ and initially increases as the impact parameter ρ is increased. Φ increases to a maximum value, then decreases to zero as ρ goes beyond the range of force. In the point Coulomb potential the scattering angle Φ also begins with π for $\rho=0$ but decreases monotonically to zero with increasing ρ.

In actual calculation the integration is done for t from 0 to a maximum value so that the contribution from the orbit corresponding to larger t can be omitted. Before doing the integration over impact parameters ρ, a coordinate transformation from the 0-x_0,z_0 to the 0-x_1,z for each orbit is needed to obtain a correct result for the angular distribution. For calculations for only the spectrum, this coordinate transform is not necessary. Keeping in mind that $\ddot{d}_{x0}$ is imaginary and $\ddot{d}_{z0}$ is real, and that we need the square of the modulus of the components, we have

$$|\ddot{d}_z(k)|^2=|\ddot{d}_{z0}(k)|^2\cos^2\psi_0+|\ddot{d}_{x0}(k)|^2\sin^2\psi_0 \ , \tag{26}$$

where ψ_0 is the angle between the 0-z axis and the 0-z_0 axis. This angle is determined by the orientation of the symmetry axis of an orbit and thus is a function of impact parameter. The doubly differential cross section is then obtained by numerical integration of Eqs. (6) and (7). The computing time mostly depends on the number of impact parameters. Not all values of the impact parameter ρ are equally important. The significant values of ρ are limited within a certain range depending on Z, T_1, k/T_1, and the potential. The code chooses automatically the proper impact parameters to minimize both the numerical error and the computing time.

To determine the numerical accuracy of the code we compared our results for trajectories and their Fourier transforms with known results, such as the Coulomb trajectory. We also compared our results for both spectra and angular distributions with other calculations. Precise comparison was made between our numerical results and results obtained from the analytic Coulomb formulas Eq. (30). For the point Coulomb potential, within $T_1=10$ eV–100 keV and $Z=2$–92, these results agree with each other within 1%. Outside this range the numerical error becomes slightly larger. The useful energy range depends on the atomic number of the target element. For light elements, like aluminum ($Z=13$), accurate results can be obtained for energies down to 0.1 eV. This is not true for high-Z elements. On the other hand, the high-energy endpoint can go up to several MeV for $Z=92$. This behavior can be characterized by the quantity $\nu=Z\alpha/\beta$. For $\nu=0.1$–150, the code gives less than 2% error in general. Further tests have been made by comparing the results from CLB with some available quantum-mechanical numerical calculations for screened potentials. In the

low-energy range in which we expect classical results are valid, our results agrees with others[18,19] within a few percent. Because of the differences in the methods, we do not expect precise agreement. We also tested our code for the high-frequency limit. Here we mean by the high-frequency limit the limit of the classical bremsstrahlung spectrum as $k/T_1 \to \infty$. Of course, this is beyond the physical limit of the real situation. According to Kogan and Kukushkin,[20] the high-frequency limit of classical bremsstrahlung given by Kramers for the point Coulomb potential will not be changed by the existence of screening. Our results confirm this conclusion. For $Z=13$ and $T_1=1$ eV, the cross section $\sigma=[(\beta/Z)^2]kd\sigma/dk$ obtained with the CLB code reached the Kramers's value $\sigma=5.605$ mb at $k/T_1=10^6$ while within the normal range of the spectrum ($k/T_1=0$–1) the cross section is of the order of 10^{-3} mb.

The numerical error of the CLB code mainly comes from the following sources: (i) limited accuracy of interpolation of the numerical potential especially at large distances, (ii) the finite number of impact parameters utilized in integrating over the beam, and (iii) numerical Fourier-transform methods. Further improvement of the code to increase the numerical accuracy is possible if necessary.

III. RESULTS FOR SPECTRA

A. Dependence on impact parameter

As defined in Sec. II, $A_1(\rho)$ characterizes the radiation intensity from electrons with impact parameters between ρ and $\rho+d\rho$. For a fixed value of k/T_1, $A_1(\rho)$ is a function of ρ. Figure 3 shows the dependence of $A_1(\rho)$ on the impact parameter ρ, for fixed values of k/T_1, for $Z=13$ and $T_1=150$ and 50 eV.

In the point Coulomb case, $A_1(\rho)$ can be obtained analytically:[14]

$$A_1(\rho)=\frac{2\pi^3k^2Z^2}{3T_1^2}\rho\left[\left|H_{i\mu}^{(1)'}(i\mu\epsilon)\right|^2+\frac{\epsilon^2-1}{\epsilon^2}\left|H_{i\mu}^{(1)}(i\mu\epsilon)\right|^2\right], \quad (27)$$

where $H^{(1)}$ and $H^{(1)'}$ are the Hankel function and its derivative with respect to the argument, ϵ is the eccentricity of the orbit, related to the impact parameter by

$$\epsilon=(1+4T_1^2\rho^2/Z^2\alpha^2)^{1/2}, \quad (28)$$

$\mu=\nu_1 k/2T_1$, $\nu_1=Z\alpha/\beta$ with β the incident electron velocity, Z is the atomic number of the target element, and α is the fine-structure constant. The limiting values, as functions of the impact parameter, are

$$A_1(\rho\to 0)=0, \quad A_1(\rho\to\infty)=0. \quad (29)$$

For the screened case, the limiting values of $A_1(\rho)$ for $\rho=0$ and $\rho=\infty$ are the same as in the point Coulomb case. Only a certain range of impact parameters contribute significantly to the radiation. In the point Coulomb case, for a fixed μ, A_1 is a function of the combined variable $\gamma=(2T_1\rho/Z\alpha)^2$ [note: $\epsilon=(1+\gamma)^{1/2}$]. Figure 4 shows on a semilog scale A_1 versus γ for various values of μ. The curves in Fig. 4 are normalized so that $\int A_1 d\gamma=1$. We find that for μ from 0.01 to 2 the peaks of A_1 occur for about $\gamma=1$. With screening this effective range involves smaller γ (i.e., closer to the origin) and the

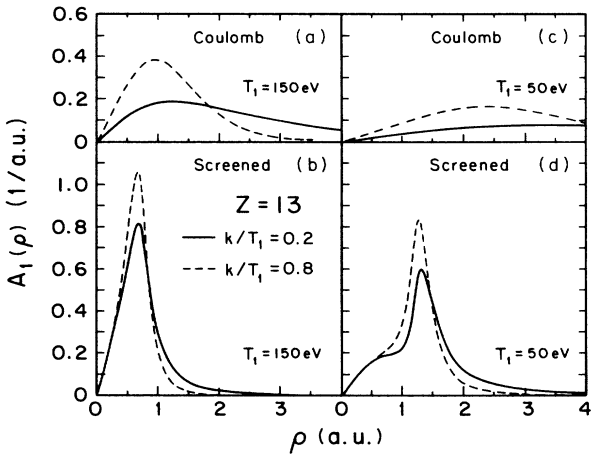

FIG. 3. $A_1(\rho)$ for fixed k/T_1 as functions of the impact parameter ρ for $Z=13$, $k/T_1=0.2$ and 0.8. (a) For $T_1=150$ eV, point Coulomb potential; (b) for $T_1=150$ eV, screened potential; (c) for $T_1=50$ eV, point Coulomb potential; (d) for $T_1=50$ eV, screened potential.

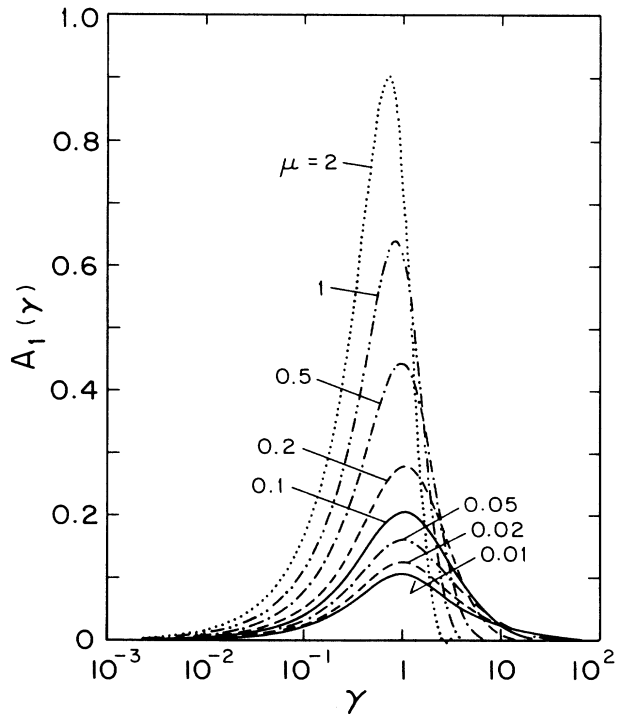

FIG. 4. $A_1(\rho)$ as functions of $\gamma=(2T_1\rho/Z\alpha)^2$ for fixed $\mu=\frac{1}{2}(k/T_1)(Z\alpha/\beta)$ for the point Coulomb potential. A_1 is normalized so that $\int A_1 d\gamma=1$.

curves are more narrowly peaked. Due to the fact that potential drops faster than in the point Coulomb case, the contribution from scattering in outer orbits is less important. For a given potential the location of the peaks depends on the electron energy. For high incident electron energy, more of the radiation comes from small impact parameters (the peak is close to the nucleus) while for low-energy electrons are more of the radiation comes from larger impact parameters.

B. Features of spectra

(1) The point Coulomb case. An analytic expression for the classical Coulomb bremsstrahlung spectrum was obtained by Kramers:[4]

$$\sigma_{CC}=\frac{4\pi^2\alpha^3}{3}i\mu H_{i\mu}^{(1)}(i\mu)H_{i\mu}^{(1)'}(i\mu)\ . \tag{30}$$

Here the reduced cross section $\sigma=(\beta^2/Z^2)kd\sigma/dk$. The subscript CC denotes the classical Coulomb case, while we will use CS for the classical screened case. Tabulation of σ_{CC} as a function of μ can be found in Ref. 12. Figure 5 shows the results for the classical Coulomb bremsstrahlung spectrum evaluated from Eq. (30) for $Z=13$ and $T_1=1$ eV-1 MeV. For the Coulomb potential the three variables Z, T_1, and k/T_1 appear only in the single combination μ. All the curves of Fig. 5 are in fact the same curve and will coincide if plotted against $\mu=\nu_1 k/2T_1$ rather than k/T_1. Expansions for two important limiting situations have been derived from Eq. (30):

$$\sigma_{CC}=\frac{16\alpha^3}{3}\left[(1+\pi\mu)\ln\left[\frac{2}{\gamma\mu}\right]+O(\mu^2)\right],\quad \mu\ll 1 \tag{31}$$

$$\sigma_{CC}=\frac{16\pi\alpha^3}{3^{3/2}}[1+d_1\mu^{-2/3}+d_2\mu^{-4/3}+2d_1d_2\mu^{-2}+O(\mu^{-8/3})],\quad \mu\gg 1\ , \tag{32}$$

where $\gamma=e^C=1.781\,07$, $C=0.577\,21$ is the Euler's constant, $d_1=0.217\,741$, $d_2=-0.013\,121\,4$. Equation (31) and the first two terms of Eq. (32) were given by Kramers;[4] the remaining terms of Eq. (32) were obtained by Florescu and Costescu.[12]

Consider first the hard photon region. Equation (32) says that in the $\mu\gg 1$ region the asymptotic value of the spectrum is $\sigma=16\pi\alpha^3/3^{3/2}=5.61$ mb. For low energies, $\mu\gg 1$ in the hard photon region and the spectrum is flat. For high energy, μ is small and the tip value is still far larger than the Kramers value.

In the soft photon region, all curves of Fig. 5 diverge logarithmically as k/T_1 goes to zero. For fixed k/T_1, the cross section decreases with decreasing incident electron kinetic energy but never drops below the Kramers values, i.e., the Gaunt factor of the classical Coulomb spectrum is always bigger than 1. For fixed T_1, the Gaunt factor increases with decreasing value of k/T_1 and goes to infinity when $k/T_1\to 0$. However, the integral of the energy spectrum over k/T_1 from 0 to 1 (which is the integrated energy-loss cross section) does not diverge.

(2) Screened case. For a screened potential the spectrum is generally a function of all three variables Z, T_1, and k/T_1.[21] Spectra do not scale and have to be calculated for individual cases. In Fig. 6 we present the classical screened (CS) results for spectra for $Z=13$ and 79. The following features are different from the Coulomb case.

(1) The logarithmic divergence of the spectrum at the soft photon end point no longer occurs. This is due to the fact that the screened potentials for neutral atoms (in our case, the Dirac-Slater potential) are short-range potentials and the integration of the radiation intensity over impact

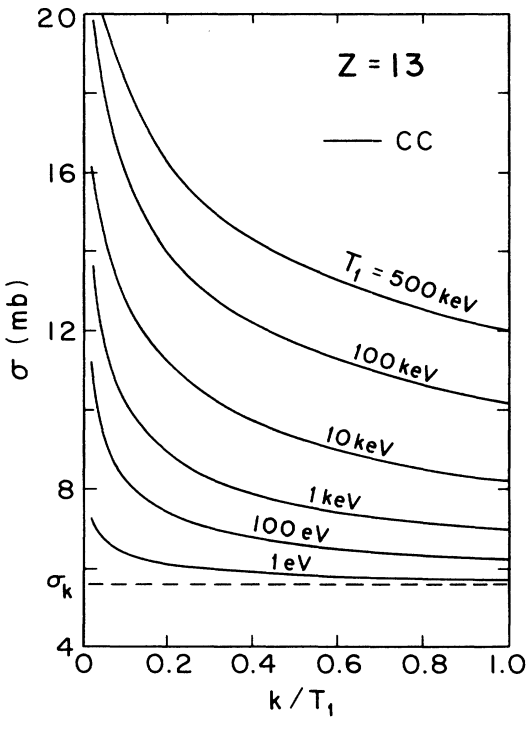

FIG. 5. Classical bremsstrahlung spectra for point Coulomb potential for $Z=13$ and T_1 from 1 eV to 500 keV. The dashed horizontal line indicates the Kramers value $\sigma=5.61$ mb.

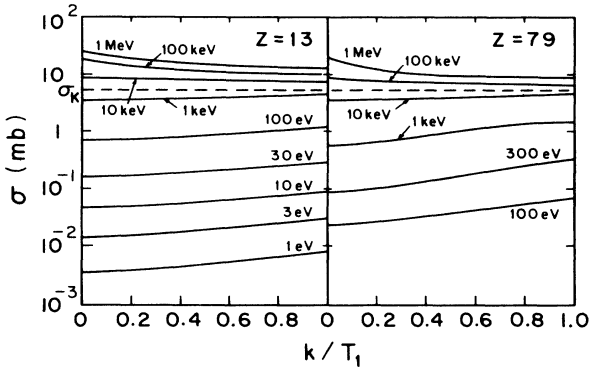

FIG. 6. Classical bremsstrahlung spectra for screened potentials (a) for $Z=13$, (b) for $Z=79$. The dashed horizontal line indicates the Kramers value $\sigma=5.61$ mb.

parameters converges.

(2) Cross sections are reduced from the Coulomb results. Screening becomes increasingly important with decreasing electron energy T_1. The Kramers value is no longer the lower limit of the spectrum. The Gaunt factors are smaller than 1 for low electron energy (below about 20 keV in the case of gold and 1 keV in the case of aluminum). For very low energies the spectrum drops almost linearly with energy.

(3) For fixed T_1, the spectrum for a low T_1 increases with k/T_1 while the spectrum for a high T_1 decreases with k/T_1. In either case the trend is to reach the Kramers value. It is predicted[20] that, in screened potentials, the high-frequency limit $\sigma(k\rightarrow\infty)$ remains the same as in the point Coulomb case, i.e., the spectra for all energies reach the same value $\sigma=5.61$ mb when $k/T_1\rightarrow\infty$. The argument is that from the classical theory of electromagnetic radiation, very-high-frequency radiation is associated with very high angular velocity of the electron motion. This very high angular velocity is possible only for electron orbits very close to the center of scattering, where the potential is like the Coulomb potential. In Fig. 7 we show the asymptotic behavior of the classical bremsstrahlung spectrum in a screened potential up to ultrahigh frequencies, obtained with our numerical code. These results confirm that the high-frequency limit does not change in the case of a screened potential. Note however that this high-frequency limit will not be correct if the screened potential does not have Coulombic behavior at the origin, i.e., the prediction is valid only for point, not structured, nuclei.

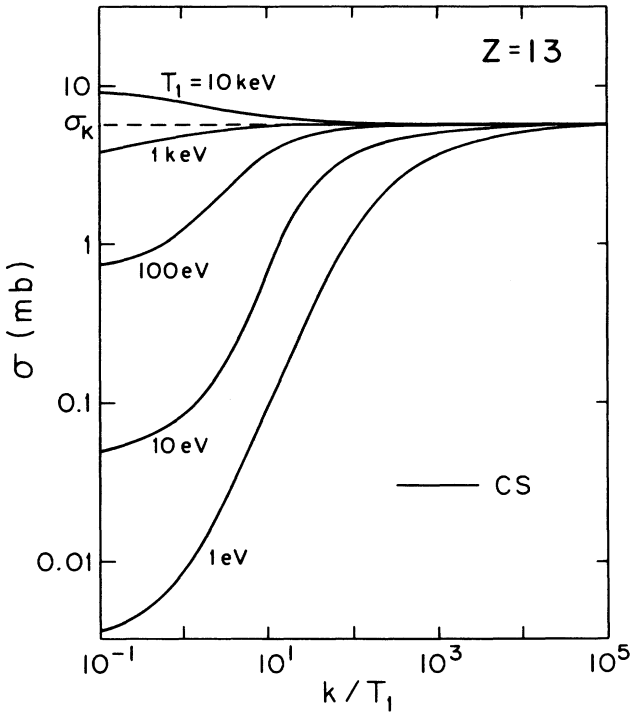

FIG. 7. Classical bremsstrahlung spectra in a screened Coulomb potential, showing (unphysical) high-frequency behavior. Spectra are shown as functions of k/T_1 for $Z=13$ and for T_1 between 1 eV and 10 keV. All curves asymptotically approach the Kramers value when $k/T_1\rightarrow\infty$.

C. Validity of classical predictions for spectra

(1) The point Coulomb case. The validity of classical results for bremsstrahlung spectra in the point Coulomb potential has been studied, for example, by Florescu,[12] Feng,[9] and others. According to Feng's work,[9] the region of validity in electron and photon energy can be characterized by a single parameter $\eta=\nu_1(1-k/T_1)$. For $\eta>0.7$, classical results for the Coulomb potential case agree with nonrelativistic quantum-mechanical results in the same potential within 5%. Figure 8 illustrates the region of validity of classical results with respect to Sommerfeld's nonrelativistic quantum dipole approximation calculation for the same potential.

Comparisons with accurate numerical partial-wave results are also available.[9] Figure 8 also shows the region of validity of the classical results with respect to the exact partial-wave results (EC) in the point Coulomb potential. While the characteristic nonrelativistic Coulomb variables are ν_1 and k/T_1, for the exact partial-wave calculation the dependence of σ on the three variable T_1, Z, and k cannot be reduced. Thus the region of validity also depends on the atomic number Z.

We see from Fig. 8 that for large ν_1 and small k/T_1 (low energy and soft photons) the classical method generally correctly predicts the bremsstrahlung spectrum. For very large ν_1 this validity extends to the entire spectrum.

(2) Screened case. Figure 9 shows the comparison of the classical screened results (CS) with the relativistic partial-wave screened results (ES). Data for quantum-

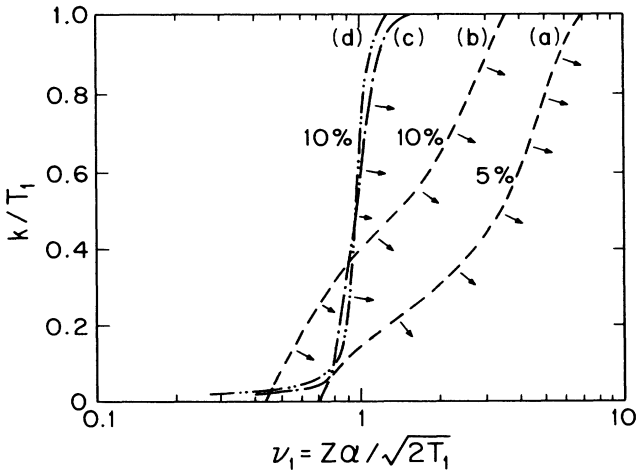

FIG. 8. Region of validity of classical results for bremsstrahlung spectra in the point Coulomb potential. Curves shown are the boundaries of the region in which the classical results have errors less than the specified percentage in comparison with (a) and (b) the nonrelativistic quantum dipole method (Sommerfeld formula), (c) and (d) the exact relativistic partial-wave multipole expansion method, (c) for $Z=74$ and (d) for $Z=26$.

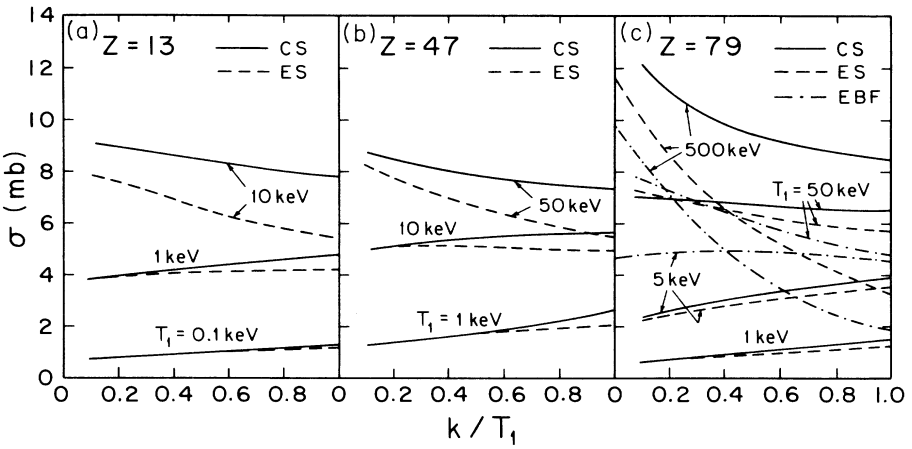

FIG. 9. (a) Comparison of classical screened (CS) results with "exact" screened (ES) results, showing bremsstrahlung spectra for $Z=13$, $T_1=0.1$, 1, and 10 keV. (b) Same as (a) but for $Z=47$, $T_1=1$, 10, and 50 keV. (c) Same as (a) but for $Z=79$, $T_1=1$, 10, and 50 keV and also includes comparisons with EBF results.

mechanical results for $T_1=0.1$ keV are from nonrelativistic dipole calculations.[18,19] Figure 9(c) also includes comparisons with Elwert-Born form-factor results (EBF). For fixed T_1, the agreement of CS results with ES results is better in the soft photon region. With decreasing electron energy the region of validity can extend over the entire spectrum (k/T_1 from 0 to 1) with better than 10% accuracy. The upper limit of the electron energy for which the classical method is valid for a reasonably wide range of the spectrum depends on the atomic number of the target element. For a high-Z element, like gold ($Z=79$), CS results agree with ES results within 10% error for the electron energies up to 50 keV, while for aluminum ($Z=13$) this limit drops to about 1 keV, and for silver ($Z=47$) 10 keV. Evidently there is still some scaling of energy with respect to the atomic number, roughly of the T_1/Z^2 type which exists in the point Coulomb case.[21]

At this time we are not able to provide a comparison of CS results with ES results for electron energies lower than 100 eV due to the unavailability of ES data in this energy range. However, as we see from Fig. 9, the tendency of better agreement towards the lower energy suggests that the classical results will be valid for energies lower than 100 eV, at least to some extent. Accurate data for low-energy spectra from quantum-mechanical calculations are still needed to make direct comparisons. In analytic approaches the atomic form-factor method is often used to predict bremsstrahlung spectra for screened potentials. However, the form-factor method, based on Born approximation, is good only for relatively high electron energies and light elements. For example, for $Z=79$, $T_1=5$ keV, the Elwert-Born form-factor method gives 30%–100% error.[9] Our present numerical classical results give far less error (4% at the soft photon endpoint and about 10% in the hard photon region). The classical numerical method also takes much less computer time than a full numerical partial-wave quantum-mechanical calculation.

With increasing electron energy the discrepancy between classical results and partial-wave results increases, both in the Coulomb potential and in screened potential cases. However, we have found that the ratio between Coulomb results and screened results, predicted classically, remains close to that of the full quantum-mechanical calculation (Table I). This indicates that the screening factor (defined as the ratio of screened to Coulomb results), found classically, can be used together with quantum Coulomb results to obtain useful predictions. Figure 10 shows the spectra σ_1 obtained in this way compared with the form-factor results for $Z=79$ at $T_1=50$ and 500 keV. In this example, our results have substantially better accuracy than the Elwert-Born form-factor results. Our method in this case needs accurate Coulomb data to begin with. However, in many cases, it is easier to obtain a Coulomb result than a screened one. While the atomic form-factor method is good for sufficiently high energies, it does require calculation of triply differential cross sections.

It should be recognized that the classical method fails to predict some quantum-mechanical aspects of radiation, related to density of states effects, such as the deep suppression of the quantum spectrum at the tip, which comes from the reduced normalization (small distance magnitude) of the outgoing low-energy electron continuum waves in a screened potential, as well as the existence of the tip cutoff.

IV. ANGULAR DISTRIBUTION OF CLASSICAL BREMSSTRAHLUNG

A. Results for the asymmetry parameter

For the point Coulomb potential the asymmetry parameter of the angular distribution of classical bremsstrahlung, like the spectrum, is determined by the single parameter μ, i.e., $a_2=a_2(\mu)$. The function a_2 can be given as an analytic expression in terms of hypergeometric functions.[22] A numerical tabulation of this function is also available.[22] The dependence of a_2 on μ is illustrated in Fig. 11. As we can see, a_2 is a smooth monotonic function of μ. The limiting values are $a_2\rightarrow 1$ for $\mu\rightarrow 0$ and

TABLE I. Comparison of CC, CS, EC, and ES results for bremsstrahlung spectra. Numbers given are the reduced cross sections $\sigma=(\beta^2/Z^2)kd\sigma/dk$ in millibarns. CC, classical Coulomb; CS, classical screened; EC, exact Coulomb; ES, exact screened. The last column shows the ratios of the screening factors.

			$\sigma=(\beta^2/Z^2)kd\sigma/dk$ (mb)				
Z	T_1 (keV)	k/T_1	CC	CS	EC	ES	$(\sigma_{CC}/\sigma_{CS})/(\sigma_{EC}/\sigma_{ES})$
13	1.0	0.1	10.15	3.82	9.98	3.77	1.01
		0.4	7.90	4.23	7.35	3.99	1.01
		0.6	7.44	4.46	6.77	4.06	1.00
		0.8	7.16	4.65	6.40	4.13	0.99
		1.0	6.94	4.79	6.16	4.17	0.98
	10.0	0.4	9.72	8.61	7.77	6.89	1.00
		0.8	8.55	7.99	6.28	5.83	0.99
		1.0	8.23	7.78	5.82	5.49	0.99
	50.0	0.1	14.88	13.10	11.20	9.46	0.96
		0.2	13.04	12.27	9.08	8.35	0.98
		0.4	11.37	11.07	6.86	6.65	1.00
		0.6	10.48	10.32	5.50	5.46	0.99
		0.8	9.90	9.80	4.56	4.55	1.01
		0.9	9.68	9.59	4.17	4.17	0.99
79	10.0	0.6	6.86	4.45	6.73	4.16	0.95
		0.8	6.66	4.61	6.50	4.26	0.95
		0.9	6.59	4.67	6.41	4.30	0.95
	50.0	0.1	10.46	6.89	10.80	7.14	1.01
		0.2	9.14	6.90	9.30	6.92	0.99
		0.4	8.09	6.74	7.95	6.42	0.97
		0.6	7.60	6.60	7.26	6.03	0.96
		0.8	7.29	6.50	6.78	5.77	0.96
		1.0	7.09	6.42	6.45	5.59	0.96
	500.0	0.5	9.58	9.33	6.07	5.64	0.95
		0.9	8.59	8.44	3.83	3.53	0.94
		1.0	8.44	8.30	3.43	3.13	0.93

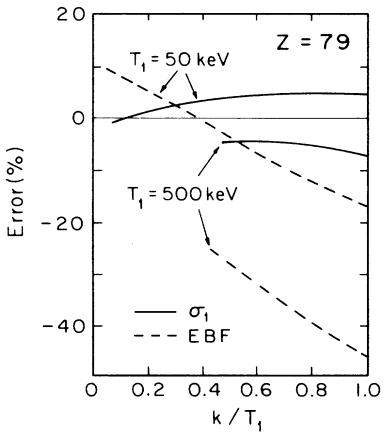

FIG. 10. Errors of bremsstrahlung spectra for screened potential as predicted by multiplying the ratio of screened to Coulombic results calculated from the classical method by the exact Coulomb results, as compared with corresponding errors of Elwert-Born form-factor (EBF) predictions.

$a_2\to -1$ for $\mu\to\infty$.

In Fig. 12 we illustrate the shape function as a function of angle for several different values of a_2. When $a_2=1$ more radiation is emitted in the direction of the incoming

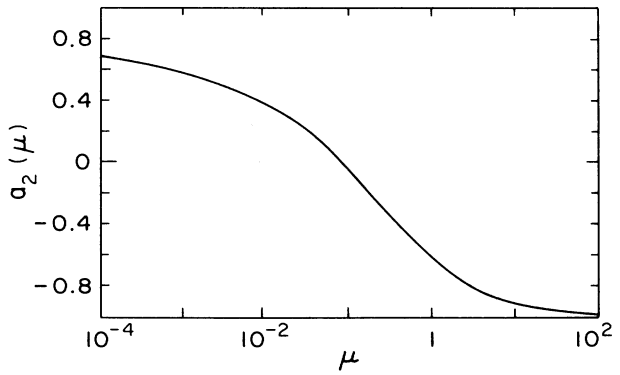

FIG. 11. The asymmetry parameter for classical Coulomb bremsstrahlung spectra as a function of $\mu=\frac{1}{2}(Z\alpha/\beta)(k/T_1)$ based on data from Ref. 22.

electron beam, while $a_2=-1$ implies more radiation in the direction perpendicular to the beam. For $a_2=0$, there is isotropic radiation. The case $a_2\to 1$ corresponds to small values of μ and thus high electron incident energy and/or low photon energy, while $a_2\to -1$ corresponds to low electron energy at fixed k/T_1.

In the screened Coulomb potential the angular distribution is still determined by the asymmetry parameter. However, in this case the dependence of the asymmetry parameter on Z, T_1, and k cannot be simplified to a one variable function $a_2=a_2(\mu)$. With screening, the value of a_2 can be lower than -1, the Coulomb limit. In Fig. 13 we show a comparison of values of a_2 $(Z,T_1,k/T_1)$ for the point Coulomb potential [classical coulomb results (CC)] and a screened potential (classical screened results) for $Z=13$ and T_1 from 1 eV to 500 keV. The behavior of the screened results for a_2 can be classified into the following three regions.

(A) For high-energy (above 10 keV in this example), CS results are basically the same as CC results except in the soft photon region of the spectrum, in the example for $k/T_1=0.2$. The screening effect is negligible for high-energy scattering except in the soft photon region.

(B) In the medium-energy region screening effects become important. CS results are below CC results (more negative). However, the pattern of change remains similar to the CC results.

(C) In the low-energy region (below 150 eV in this example) the values of a_2 change dramatically with the electron energy, showing some oscillation in energy, similar in character for all k/T_1.

We have also obtained similar results for the $Z=79$ case. In this case the large changes of a_2 occur at higher energy. The value of a_2 reaches a minimum when T_1 is about 1 keV. It starts to increase as T_1 continue to decrease, reaching a peak at about $T_1=300$ eV, and then begins to decrease again.

These features can be understood by considering the behavior of the individual scattering trajectories of the electrons in the beam. Each electron has its own orbit determined by its impact parameter. Observed quantities, for example, the angular distribution of the radiation, are integrated results over angular distributions from individual electrons in the beam.

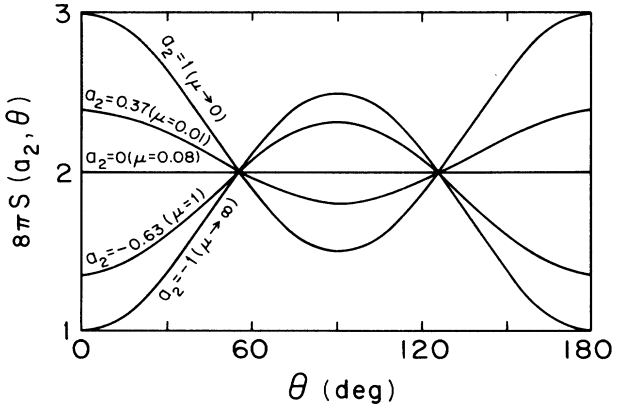

FIG. 12. The shape functions of classical bremsstrahlung spectra, as a function of the emission angle with respect to incoming electron direction, for several values of the asymmetry parameter a_2. Numbers in parentheses are the corresponding values of μ in the point Coulomb case.

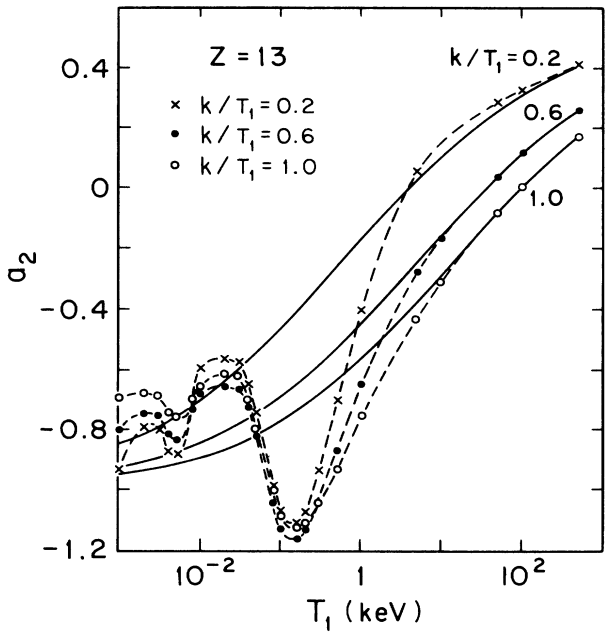

FIG. 13. Asymmetry parameter a_2 of classical bremsstrahlung spectra for the neutral aluminum atom, as a function of incident electron energy, compared with the point Coulomb results. Solid lines are for the point Coulomb results; dashed lines marked with symbols are for neutral atoms results. Three values of k/T_1 are illustrated.

The angular distribution of a subline (a subline is the spectrum of radiation associated with given impact parameter as a function of k/T_1) can be expressed in the same way as for the spectrum, by a parameter $a(\rho)$, the asymmetry parameter for the subline. Namely,

$$\frac{kd^2\sigma}{dkd\Omega}=\int_0^\infty d\rho\, A_1(\rho)\left[1+\frac{a(\rho)}{2}P_2(\cos\theta)\right] . \tag{33}$$

From Eqs. (5)–(9), we find that

$$a(\rho)=(\ddot{\mathbf{d}}_k^2-3\ddot{d}_{kz}^2)/\ddot{d}_k^2 . \tag{34}$$

The asymmetry parameter of the resulting spectrum (obtained by integration) can be expressed in terms of an integration of the asymmetry parameter weighted by the magnitude of the subline, i.e.,

$$a_2(Z,T_1,k)=\frac{1}{A}\int_0^\infty d\rho\, A_1(\rho)a(\rho) , \tag{35}$$

with

$$\frac{1}{A}\int_0^\infty A_1(\rho)d\rho=1 . \tag{36}$$

In the point Coulomb case both $A_1(\rho)$ and $a(\rho)$ change smoothly with impact parameter, as we see from Figs. 14(a) and 14(b) which shows $a(\rho)$ and $A_1(\rho)$ as functions of ρ for fixed k/T_1 at two different energies $T_1=150$ eV

and $T_1=50$ eV. We find that the $a(\rho)$ curve for $T_1=50$ eV is lower than that for $T_1=150$ eV for all values of ρ in the effective range. We mean by effective range that range of ρ within which $A_1(\rho)$ has significant magnitude. In Fig. 14 the $A_1(\rho)$ curves are all normalized so that $\int A_1(\rho)d\rho=1$.

The energy dependence of the $a(\rho)$ curves leads to the energy dependence of the integrated asymmetry parameter a_2. The energy dependence of the $a(\rho)$ curve can be understood qualitatively by the following argument. The radiation from a given trajectory mainly comes from the part of the trajectory close to the scattering center (where the maximum acceleration occurs). A small region of the trajectory near the symmetry axis 0-z_0 plays an important role. In this region the vector $\ddot{\mathbf{d}}$ mainly lies along the z_0 direction, thus the maximum radiation is in the direction perpendicular to the z_0 axis since the radiation intensity is proportional to $(\ddot{\mathbf{d}}\times\mathbf{n})^2=\ddot{\mathbf{d}}_k^2\sin^2\theta$. The x and z components of this radiation will depend on the angle ψ_0. For $0<|\psi_0|<\pi/2$, the smaller ψ_0 is, the less radiation will be in the z direction. In the point Coulomb potential, for the same impact parameter, a lower-energy electron has a larger scattering angle (Φ close to π, ψ_0 close to 0) and therefore produces less radiation in the z direction. This, as we can see from Fig. 12, corresponds to lower values of the asymmetry parameter.

For a screened potential, in the high- and medium-energy range, the energy dependence of the subline asymmetry parameter is similar to the point Coulomb case. With decreasing energy the value of $a(\rho)$ for a given ρ decreases. Hence the integrated value a_2 also decreases. However, in the screened potential case the values of a_2 are more reduced than in the point Coulomb case. This can be explained by the behavior of the scattering angle. In a screened potential, when the impact parameter ρ increases from 0, unlike in the point Coulomb case, the scattering angle does not begin to decrease immediately from the starting value π. Instead, it increases with increasing impact parameter, reaches a maximum value at a certain impact parameter, and then decreases back to π. After that it continues to decrease with increasing impact parameter until it reaches the minimum value 0. The maximum scattering angle depends on the electron energy. Except for very low energy, the maximum scattering angle is just slightly larger than π. The large scattering angles around π are related to small values of ψ_0 and therefore low values of $a(\rho)$.

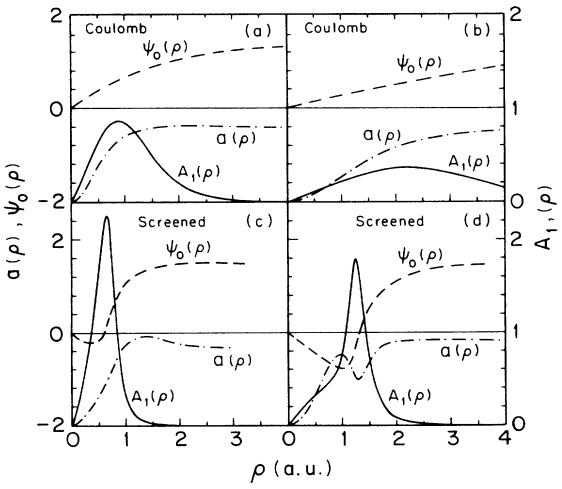

FIG. 14. Radiation intensity $A_1(\rho)$ of a given impact parameter ρ, the corresponding asymmetry parameter $a(\rho)$, and the angle ψ_0 of the symmetry axis of the trajectory, as functions of the impact parameter ρ for $Z=13$, $T_1=150$ and 50 eV, (a) and (b) for the point Coulomb potential, (c) and (d) for screened potentials.

In Figs. 14(c) and 14(d) we show $A_1(\rho)$, $a(\rho)$, and ψ_0 versus ρ for the screened potential of the aluminum atom ($Z=13$). We see, in the $T_1=150$-eV case [Fig. 14(c), compared to the point Coulomb case (Fig. 14(a)], that ψ_0 is restricted to have a smaller value within the important range of ρ. This causes the $a(\rho)$ curve to have a much lower value than the corresponding curve for the point Coulomb case. Generally speaking, in a screened potential, due to the large scattering angles of the trajectories with the important impact parameters, the asymmetry parameters of sublines associated with these trajectories are reduced from the corresponding value of the point Coulomb case. Therefore, the integrated asymmetry parameter has a lower value for the screened potential.

Now, let us discuss the oscillation of a_2 which we have seen in Fig. 13. With decreasing energy, the maximum value of the scattering angle become much larger than π. The corresponding values of ψ_0 are no longer small. For example, for $T_1=50$ eV, as shown in Fig. 14(d), $|\psi_0|$ can be as big as $\pi/4$ at about $\rho=1$ a.u. Remembering that a larger value of ψ_0 corresponds to a higher value of $a(\rho)$, we see a peak of $a(\rho)$ at about the same distance. The high value of $a(\rho)$ around $\rho=1$ a.u. has a great contribution to the integrated result because it occurs in the important range of ρ. Compared to the $T_1=150$-eV case [Fig. 14(c)], it is obvious that the integrated asymmetry parameter for $T_1=50$ eV has a higher value, as we have already seen in Fig. 13.

For even lower energies, the maximum scattering angle can be very large (even several times π). When the scattering angle increases from 0 to the maximum and decreases back to 0, the corresponding value of ψ oscillates. This oscillation causes $a(\rho)$ to oscillate correspondingly. Further, because of the low energy, the intensity curve $A_1(\rho)$ is more narrowly peaked, with a position moved outwards. Because of the narrow peak of the $A_1(\rho)$ curve, the oscillations of $a(\rho)$ are unlikely to be averaged by the integration. The actual value of a_2 is determined by a combination of these factors, namely which part of the oscillating $a(\rho)$ falls in the dominant range of ρ. Lowering electron energy, the peak of the $A_1(\rho)$ curve moves outward and $a(\rho)$ oscillates more rapidly with ρ. The highs and the lows of $a(\rho)$ enter the important region of ρ alternatively. The result of these changes is the oscillation of the integrated a_2. All these discussions of the asymmetry parameter are based on the ideas of the classical theory. We have not attempted to formulate a corresponding quantum theory, and it is not clear whether similar features would persist.

B. Validity of classical angular distributions

The validity of the classical predictions for the bremsstrahlung angular distribution should be examined separately from the validity of spectrum predictions, as it further clarifies the validity of the classical method. The asymmetry parameters calculated from the classical method and from the quantum-mechanical method has been compared by Florescu *et al.*[22] for the point Coulomb case. The classical results are good for large values of ν_1 and small values of k/T_1, as in the case of the spectrum. However, the region of validity for the asymmetry parameter is more restricted to the larger values of ν_1 than it was for the spectrum. For example, for $\nu_1=20$ and $k/T_1=0.2$ the relative error of classical results for the asymmetry parameter is about 7%, while for the spectrum it is less than 2%.

The relative error of classical results for the shape function can be estimated from the relative error of the asymmetry parameter:

$$\frac{\delta S}{S}=\frac{a_2P_2(\cos\theta)}{2+a_2P_2(\cos\theta)}\left[\frac{\delta a_2}{a_2}\right]. \tag{37}$$

The absolute value of the multiplier in Eq. (37) is smaller than one for all possible values of θ and a_2. This means that the shape function has less relative error than the asymmetry parameter. Figure 15 shows the numerical values of the multiplier as functions of θ for some selected values of a_2. Except for $a_2\to -1$, which corresponds to infinitely large μ, and $\theta<30°$ or $\theta>150°$, the absolute value of the multiplier is smaller than 0.3. In these cases, the agreement of classical results with quantum results for the shape function is better than for the asymmetry parameter by a factor of 3 or more. (We do not show, in Fig. 15, the cases when $a_2>0$, since they are related to small values of ν_1, and the classical method is not valid anyway.)

For the screened case the validity of the classical results for the angular distribution of bremsstrahlung radiation can be obtained by comparisons with quantum results, as we did for the spectrum. In Fig. 16 we show comparisons

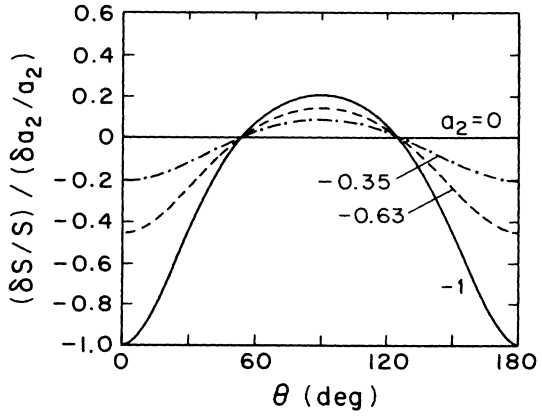

FIG. 15. Ratio of relative error of the shape function to relative error of asymmetry parameter a_2 as a function of θ for several values of a_2.

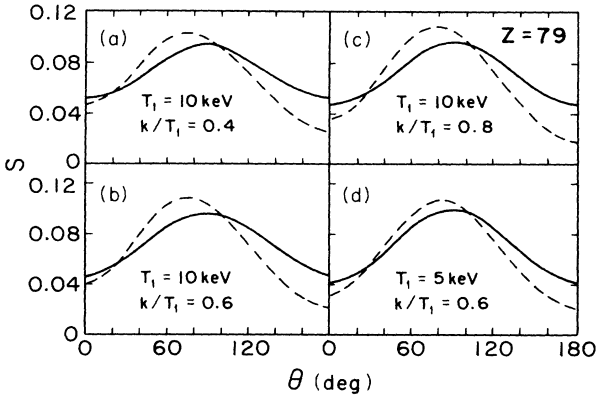

FIG. 16. Comparison of CS (solid lines) and ES (dashed lines) results for the shape function for $Z=79$, $T_1=5$ and 10 keV. The ES results include contributions from higher multipole radiation and therefore are not symmetric about $\theta=90°$.

of the shape function for Au obtained with the classical numerical method and with the exact partial-wave method. The results from the exact partial-wave method include contributions from higher multipole radiation and so do not have the symmetry which exists in the dipole radiation case. However, from the comparison with the ES results we still can get some idea about the validity of the classical method. For $Z=79$, $T_1=10$ keV, $k/T_1=0.4$, 0.6, and 0.8 the discrepancy between the classical results and the ES results is about 10–25 % in the $\theta=0°-180°$ range. For lower energy (see the $T_1=5$-keV case in Fig. 16) the discrepancy is smaller. The large discrepancy in the $90°<\theta<180°$ range is due to the contribution from higher multipole radiation, which we have not included in our classical calculations.

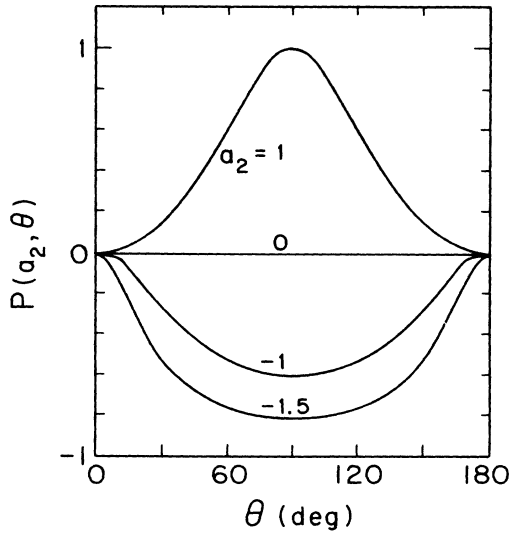

FIG. 17. Polarization degree P as a function of θ for several values of a_2.

C. Polarization

The polarization of classical bremsstrahlung in a central potential is related directly to the angular distribution of the spectrum. Once the asymmetry parameter is determined both the angular distribution and the polarization are determined [see Eqs. (11) and (18)]. $P=1$ corresponds to 100% linear polarization in the y direction. Full polarization in the x-z plane is represented by $P=-1$. If $P=0$, the radiation is not polarized. For a given a_2, the polarization degree P is a function of the angle θ.

Figure 17 shows the polarization degree versus the angle θ for four different values of the asymmetry parameter a_2. In the point Coulomb case the value of a_2 is limited to the range from -1 to 1, so $a_2<-1$ is meaningful only in the screened potential case. We see that in the forward and backward directions ($\theta=0°$ or 180°) radiation is not polarized. Maximum polarization occurs at $\theta=90°$. With $a_2=1$, the maximum polarization is 100% y polarization. In the Coulomb case the lowest value of a_2 is -1 and therefore maximum polarization is 60% in the x-z plane. If $a_2=0$, which corresponds to isotropic radiation, then P is also equal to zero and the radiation in all directions is unpolarized. Since $a_2>0$ corresponds to high incident electron energy, strong y polarization for $\theta=90°$ occurs for high-energy bremsstrahlung. Similarly the strong x-z polarization for $\theta=90°$ occurs for the low-energy (finite k/T_1) bremsstrahlung.

In the screened cases, polarization is different from the point Coulomb case because of the shift of the value of a_2. The predictions follow from the asymmetry parameter a_2 together with Fig. 17. In general, screening reduces the value of a_2. This results in more polarization in the y direction compared to the point Coulomb case. At very low energies where a_2 oscillates with energy the polarization degree will also oscillate.

ACKNOWLEDGMENTS

The authors wish to express their thanks to Dr. V. Florescu for helpful discussions. They also thank Dr. L. A. Collins and Dr. J. Scofield who provided some data which we used to test our code. This work is supported in part by the National Science Foundation under Grant number PHY-8420845.

[1]H. K. Tseng and R. H. Pratt, Phys. Rev. A **3**, 100 (1971).
[2]C. M. Lee, Lynn Kissel, R. H. Pratt, and H. K. Tseng, Phys. Rev. A **13**, 1714 (1976); R. H. Pratt and H. K. Tseng, *ibid.* **11**, 1797 (1975) (tip region); R. H. Pratt and C. M. Lee, *ibid.* **16**, 1733 (1977) (soft photon region); H. K. Tseng and R. H. Pratt, *ibid.* **19**, 1525 (1979) (high energy above 2 MeV); C. M. Lee, R. H. Pratt, and H. K. Tseng, *ibid.* **16**, 2169 (1977) (ions).
[3]R. H. Pratt, H. K. Tseng, C. M. Lee, Lynn Kissel, Crawford MacCallum, and Merle Riley, At. Data. Nucl. Data Tables **20**, 175 (1977); **26**, 477(E) (1982).
[4]H. A. Kramers, Philos. Mag. **46**, 836 (1923).
[5]A. Sommerfeld, Ann. Phys. (Leipzig) **34**, 257 (1931).
[6]G. Elwert, Ann. Phys. (Leipzig) **34**, 178 (1939).
[7]H. A. Bethe and E. E. Salpeter, *Quantum Mechanics of One- and Two-Electron Atoms* (Plenum, New York, 1977).
[8]H. A. Bethe and W. Heitler, Proc. R. Soc. London, Ser. A **146**, 83 (1934).
[9]I.-J. Feng and R. H. Pratt, University of Pittsburgh Report No. PITT-266, 1981 (unpublished).
[10]R. H. Pratt, in *Fundamental Processes in Energetic Atomic Collisions*, edited by H. O. Lutz, J. S. Briggs, and H. Kleinpoppen (Plenum, New York, 1983), p. 145.
[11]R. H. Pratt and I. J. Feng, in *Atomic Inner Shell Physics*, edited by B. Crasemann (Plenum, New York, 1985).
[12]V. Florescu and A. Costescu, Rev. Roum. Phys. **23**, 131 (1978).
[13]J. D. Jackson, *Classical Electrodynamics* (Wiley, New York, 1975).
[14]L. D. Landau and E. M. Lifshitz, *The Classical Theory of Fields*, 3rd ed. (Pergamon, New York, 1971).
[15]R. M. Thaler, M. Goldstein, and J. L. McHale, Phys. Rev. **102**, 1567 (1956).
[16]R. A. Arndt and L. D. Roper, Am. J. Phys. **51**, 418 (1983).
[17]R. A. Arndt and L. D. Roper, Am. J. Phys. **54**, 614 (1986).
[18]L. A. Collins (private communications).
[19]J. Scofield (private communications).
[20]V. I. Kogan and A. B. Kukushkin, Zh. Eksp. Teor. Fiz. **87**, 1164 (1984) [Sov. Phys.—JETP **60**, 665 (1984)].
[21]Longhuan Kim, R. H. Pratt, S. M. Seltzer, and M. J. Berger, Phys. Rev. A **33**, 3002 (1986).
[22]V. Florescu, V. Steiner, and L. Burlacu, J. Phys. B **23**, 427 (1987).